

This item is the archived peer-reviewed author-version of:

Molecular simulations for carbon dioxide capture in silica slit pores

Reference:

Kumar Mukesh, Sengupta Angan, Kummamuru Nithin Bharadwaj.- Molecular simulations for carbon dioxide capture in silica slit pores
Materials Today: Proceedings - ISSN 2214-7853 - (2023), p. 1-9
Full text (Publisher's DOI): <https://doi.org/10.1016/J.MATPR.2023.04.517>
To cite this reference: <https://hdl.handle.net/10067/2009440151162165141>

1
2 An International conference on Advances in Smart Materials, Chemical & Biochemical Engineering
3 (CHEMSMART-22)

4 Molecular simulations for carbon dioxide capture in silica slit pores

5
6 Mukesh Kumar¹, Nithin B. Kummamuru², Angan Sengupta^{1,3*}

7
8 ¹Department of Chemical Engineering, Indian Institute of Technology, Jodhpur, Rajasthan – 342030, India

9 ²Sustainable Energy Air & Water Technology, Department of Bioscience Engineering, University of Antwerp,
10 Groenenborgerlaan 171, Antwerpen 2020, Belgium

11 ³ School of Artificial Intelligence and Data Science, Indian Institute of Technology, Jodhpur, Rajasthan – 342030, India

12
13 *Corresponding Author E-mail: angan.sengupta@gmail.com
14

15 **Abstract**

16 In present work, we have performed the Grand Canonical Monte Carlo (GCMC) simulations to quantify CO₂ capture inside
17 porous silica at high operating temperatures of 673.15K and 873.15K; and over a operating pressure range of 500kPa –
18 4000kPa that are methane steam reforming process parameters. **Related chemical potential values at these thermodynamic**
19 **conditions are obtained from the bulk phase simulations in the Canonical ensemble in conjunction with Widom's insertion**
20 **technique, where the CO₂ has been accurately represented by TraPPE force field. Present structure of the** porous silica is a
21 single slit pore **geometry** of various heights (H = 20Å, 31.6Å, 63.2Å and 126.5Å), dimensions in which possible vapour-
22 liquid equilibria for generic square well fluids has been reported in literature. Estimation of the pore-fluid interactions show
23 a higher interaction between silica pore and adsorbed CO₂ compared to the reported pore-fluid interactions between
24 homogeneous carbon slit pore and adsorbed CO₂; thus resulting in an enhancement of adsorption inside silica pores of H =
25 20Å and H = 126.5Å, which are respectively **3.5** times and **1.5** times higher than that in homogeneous carbon slit pores of
26 same dimensions and at 673.15K and 500kPa. **Estimated local density plots** indicate the presence of structured layers due
27 to more molecular packing, which confirms possible liquid-like and vapour-like phase coexistence of the supercritical bulk
28 phase CO₂ under confinement.

29
30
31 **Keywords:** Carbon dioxide capture; silica pores; molecular simulations; adsorption isotherms; molecular packing.
32
33

H	Pore Height (Å)
ϕ_{ff}	Atomic pair interactions
ϵ_{ff}	Potential well depth ($k_B^{-1}\epsilon_{ff}$, K)
σ_{ff}	Collision diameter (Å)
r_{ij}	Intersite distance between two fluid atoms (Å)
ψ_{ij}	Interactions between charged sites
ϵ_0	Vacuum permittivity
ϵ_{sf}	Lennard-Jones well depth of adsorbate-fluid site interaction parameter ($k_B^{-1}\epsilon_{sf}$, K)
σ_{sf}	Effective adsorbate-fluid intermolecular diameter (Å)
q_i^γ & q_j^δ	Effective charges on molecules i and j
ρ_a	Adsorbed Density (mmol.cm^{-3})
ρ_z	Density inside pore along z-direction (mmol.cm^{-3})
T	Temperature (K)
P	Pressure (kPa)

24
25
26
27
28
29
30
31
32
33
34
35
36
37
38
39
40
41

1. INTRODUCTION

A continuous increase in the demand of energy from various sources of fossil fuels has lead to an enhanced emission of greenhouse gasses (viz. CO₂, CH₄, etc.), which results in environmental pollution and global warming. Therefore, the search for high-efficiency adsorbents for carbon dioxide (CO₂) capture is one of the most challenging problems in the energy and environmental field. Since 1970s, carbon sequestration and storage (CCS) technology has been intensively developed and tested in order to reduce CO₂ emissions into the atmosphere [1, 2]. A number of promising technologies for CO₂ capture from flue gases; including mass-transfer operations like absorption, adsorption, membrane separation, and cryogenic distillation have been studied in the recent past [3]. The most relevant technology in the post-combustion CO₂ capture is absorption processes employing aqueous alkanol-amine solutions like mono-ethanolamine (MEA) [4]. However, some of the challenges associated to the aqueous alkanol-amine based carbon capture from the gas stream are higher temperature degradation of amines, corrosion, and also, significant amount of energy requirement for solvent regeneration [5-7]. An extensive literature review shows that the adsorption technology can be a promising solution for overcoming some of the limitations associated to the chemical absorption process. Adsorption method for CO₂ capture requires the use of efficient adsorbents with high CO₂ selectivity and uptake capacity from among the gaseous mixture. Various studies on possible pure CO₂ capture at subsequently moderate thermodynamic conditions, which requires additional heat management system network and separation units in the industrial downstream and hence associated with cost penalty

1 (using porous carbon adsorbents, or porous silica-based adsorbents, or zeolites and or other surface modified metal-organic
2 frameworks (MOFs)); have been performed by different research groups [8-13].

3 Most of the **technologies described in** literature **dealing** with absorption and adsorption processes to capture CO₂ from
4 downstream processes are **applicable** at low temperature and pressure ranges. Researches on CO₂ adsorption at low to
5 moderate temperature and pressure conditions have been performed in the recent past via carbon-based materials [14-22].
6 Kirchofer et al. [14] have studied the transport properties and confinement effect of CO₂ through hydroxyl-functionalized
7 slit and step carbon pores using the non-equilibrium molecular dynamic simulations and suggested the need of different
8 transport models that can take into account the mass transfer resistances through carbon pores of various geometries. Jasuja
9 and Walton [15] conducted an experimental study on CO₂, CH₄, and water vapor adsorption on a Dimethyl Functionalized
10 UiO-66 framework and showed that presence of nonpolar functional groups is also crucial in enhancing CO₂ adsorption
11 while lowering adsorbent interactions with water. Steriotis et al. [16] performed the Grand Canonical Monte Carlo
12 (GCMC) simulations to study the adsorption phenomenon of CO₂ inside microporous carbon at 308K and 35bars. The
13 study confirms the effect of confinement on molecular packing of CO₂ molecules inside the carbon pores resulting in local
14 densification process. Balbuena and Gubbins [17] have discussed the possibility of phase transition and layering of CO₂
15 molecules inside carbon slit pore which infers sudden density fluctuation during the CO₂ capture inside carbon slit pore.
16 The structure of adsorbed CO₂ in slit-like micropores at 308K and 333K temperature and up to approximately 35bar
17 pressure has been studied by Samios et al. [18] using the GCMC simulation techniques. At these low temperatures, this
18 research shows the uptake capacity is highest in the larger pores **compared to the smaller pores**; at given pressure
19 conditions due to enhanced layering effects inside larger pores with high peak heights at the walls. Tenney and Lastoskie
20 [19] demonstrated that the CO₂ adsorption inside a graphitic slit pore has been enhanced by the heterogeneity on the pore
21 wall, compared to the homogeneous planar slit pores. Researches argued that the presence of chemical heterogeneity
22 (oxygen-containing functional groups) along with surface defects increases the active sites of the porous adsorbents for
23 CO₂ adsorption compared to the homogeneous graphitic slit pores. Lithoxoos et al. [20] had also studied the adsorption
24 capacity of pure carbon monoxide (CO), carbon dioxide (CO₂), and methane (CH₄) gases on activated carbon adsorbents at
25 298K and for pressures ranging from 0.01 to 2.0MPa and showed that the adsorption capacity of graphite increases with
26 the number of activation sites, which are generated by chemical modifications of the surface using the carboxyl and
27 hydroxyl groups. Kurniawan et al. [21] conducted GCMC simulation to study the binary mixture adsorption of CH₄ and
28 CO₂ in graphite slit pore of height 7.5 Å to 75 Å, at supercritical conditions and showed that upon increasing the pressure,
29 CO₂ has been selectively adsorbed as compared to methane inside all the graphite slit pores considered. A study by
30 Kummamuru et al. [22] on adsorption isotherms estimation of confined CO₂ inside various dimensional carbon slit pores at
31 673.15K and 873.15K over a range of loading pressure had shown that though the bulk phase CO₂ is in supercritical state,
32 however, inside the pores phase coexistence occurs due to the effect of confinement leading to layering effect of the
33 confined fluid. Authors in this study have used the Elementary Physical Model (EPM) to model the CO₂ interactions and
34 the carbon-based adsorbents are modelled using the Steele wall potential.

35 From present literature survey, as discussed above, on the CO₂ adsorption into various porous adsorbents it is evident
36 that the need of an efficient adsorbent to adsorb CO₂ at post-combustion operating conditions is essential to reduce the
37 industrial downstream energy cost penalty; which is impossible by the usage of porous carbon adsorbents as the

1 homogeneous porous carbon adsorbents show relatively low adsorption capacities for CO₂ at these post-combustion
 2 conditions. In this research, we therefore, propose to precisely quantify the CO₂ adsorption at post-combustion operating
 3 conditions inside porous silica adsorbents via the efficient molecular simulation approaches. These estimations will hence
 4 provide the crucial information for optimal process design of industrial adsorber units (pressure swing columns) with
 5 accurate number of mass transfer units and the corresponding transfer unit heights required for efficient CO₂ capture from
 6 industrial downstream. In the next section, we have described all the simulation details relevant for the present study. In
 7 section 3, results on **average bulk phase properties of CO₂**, CO₂ adsorption isotherm **data** and local density plots inside the
 8 silica slit pores have been discussed in details for better understanding of various confinement and entrance effects on
 9 adsorption mechanism and on thermodynamic phase behaviour of the adsorbate. Finally, we summarise our recent findings
 10 from the study in the conclusion section of this manuscript.

11

12 2. SIMULATION DETAILS

13

14 Estimation of the uptake capacity of an adsorbate by an adsorbent can be obtained by performing Monte Carlo
 15 simulations in the Grand Canonical ensemble, which forms the natural ensemble to estimate the uptake capacity inside any
 16 porous media [23]. In the present work, CO₂ adsorption isotherms inside porous silica adsorbents are estimated through the
 17 Grand Canonical Ensemble Monte Carlo (GCMC) simulations at temperatures of 673.15K and 873.15K within the
 18 methane steam reforming process pressure range of 500kPa to 4000kPa. **The related chemical potential to these pressure**
 19 **range and temperatures are calculated by deploying the Widom's insertion technique in conjunction to the bulk phase**
 20 **Canonical ensemble simulations.** The **three site rigid TraPPE** has been **used** to model the interactions between CO₂
 21 molecules [33, 34]. In the TraPPE force field, CO₂ molecule has been described as a linear molecule with bond length of
 22 1.160Å and rigid bending angle of 180°. **TraPPE describes the** existing van der Waals interactions between two CO₂
 23 molecules by the 12-6 Lennard-Jones (LJ) potential (equation 1). **The Lorentz-Berthelot classical mixing rule for**
 24 **estimating the potential parameters between the unlike particles has been consistent with the TraPPE force field.** All the LJ
 25 parameters for CO₂ molecules are given in Table 1.

26

$$27 \quad \phi_{ff} = 4\epsilon_{ff} \left(\left[\frac{\sigma_{ff}}{r_{ij}} \right]^{12} - \left[\frac{\sigma_{ff}}{r_{ij}} \right]^6 \right) \quad (1)$$

28 where, ϵ_{ff} is the LJ potential attractive well depth, σ_{ff} is the fluid particle collision diameter and r_{ij} is the inter-particle
 29 distance between atoms i and j, among the CO₂ molecules. The cut-off distance for the van der Waals interaction has been
 30 taken as 10Å, which is equals 3.42 σ_{ff} . The electrostatic interactions between two CO₂ molecules have been modelled by
 31 the Coulomb's Law, as shown in equation 2.

32

$$33 \quad \psi_{ij} = \left(\frac{1}{4\pi\epsilon_0} \right) \left(\frac{q_i^\gamma q_j^\delta}{r_{ij}^{\gamma, \delta}} \right) \quad (2)$$

1 Here the effective partial charges (q_i^γ and q_j^δ) on the C and O atoms of the CO_2 molecules are $+0.700e$ and $-0.350e$,
2 respectively [33], and the distance between two charges γ and δ on particles i and j is denoted by $r_{ij}^{\gamma,\delta}$ where the vacuum
3 permittivity is ϵ_0 . Using the TraPPE potential function, Isothermal-Isobaric ensemble simulations for bulk phase CO_2 has
4 been performed over a pressure range of 500kPa to 4000kPa and at temperatures of 673.15K and 873.15K. Following the
5 isothermal-isobaric ensemble simulations, the Canonical ensemble simulations at these temperatures and average volumes
6 (as calculated from the isothermal-isobaric simulations) are carried out in conjunction to the Widom's insertion technique
7 to calculate the bulk phase properties (e.g. the Radial distribution functions (RDFs), and the average Chemical potential
8 values) of CO_2 . Simulations in both Canonical and Isothermal-Isobaric ensembles are performed over 10^5 equilibration
9 cycles and 20,000 production cycles so that the standard deviations on the calculated average densities and average
10 chemical potentials are in the order of 10^{-6} and 10^{-2} , respectively. While the calculated RDFs hints at the thermodynamic
11 state of the bulk phase CO_2 (as described in the next section); the calculated average chemical potential has been used to
12 perform the Grand Canonical (GC) ensemble Monte Carlo (MC) simulations inside the porous silica.

13 Table 1: Molecular parameters used for CO_2 molecules and slit silica wall.

CO_2		Silica wall		Pore-fluid parameters	
σ_{ff} (Å)	$k_B^{-1} \cdot \epsilon_{\text{ff}}$ (K)	σ_{ff} (Å)	$k_B^{-1} \cdot \epsilon_{\text{ff}}$ (K)	σ_{sf} (Å)	$k_B^{-1} \cdot \epsilon_{\text{sf}}$ (K)
$\sigma_{\text{c-c}} = 2.8000$	$k_B^{-1} \cdot \epsilon_{\text{c-c}} = 27.00$	$\sigma_{\text{Si-Si}} = 3.3020$	$k_B^{-1} \cdot \epsilon_{\text{Si-Si}} = 9.0 \times 10^{-4}$	$\sigma_{\text{C-Si}} = 3.0510$	$k_B^{-1} \cdot \epsilon_{\text{C-Si}} = 0.1580$
$\sigma_{\text{c-o}} = 2.9250$	$k_B^{-1} \cdot \epsilon_{\text{c-o}} = 46.1800$	$\sigma_{\text{O-O}} = 3.1655$	$k_B^{-1} \cdot \epsilon_{\text{O-O}} = 78.1200$	$\sigma_{\text{C-O}} = 2.9820$	$k_B^{-1} \cdot \epsilon_{\text{C-O}} = 45.9490$
$\sigma_{\text{o-o}} = 3.0500$	$k_B^{-1} \cdot \epsilon_{\text{o-o}} = 79.00$			$\sigma_{\text{O-O}} = 3.1070$	$k_B^{-1} \cdot \epsilon_{\text{O-O}} = 78.5980$
				$\sigma_{\text{O-Si}} = 3.2330$	$k_B^{-1} \cdot \epsilon_{\text{O-Si}} = 0.2690$
				$\sigma_{\text{H-H}} = 0$	$k_B^{-1} \cdot \epsilon_{\text{H-H}} = 0.$
				$\sigma_{\text{H-O}} = 1.5820$	$k_B^{-1} \cdot \epsilon_{\text{H-O}} = 0.$
				$\sigma_{\text{H-Si}} = 1.6510$	$k_B^{-1} \cdot \epsilon_{\text{H-Si}} = 0.$
				$\sigma_{\text{H-C}} = 1.4000$	$k_B^{-1} \cdot \epsilon_{\text{H-C}} = 0.$
				$\sigma_{\text{H-O}} = 1.5250$	$k_B^{-1} \cdot \epsilon_{\text{H-O}} = 0.$

14
15 The geometry of the porous silica-based adsorbent has been represented as a single slit pore with pore height (H)
16 varying from 20Å to 126.5Å (which corresponds to $6.57 \sigma_{\text{sf}}$ to $41.56 \sigma_{\text{sf}}$). At these pore heights, researchers have already
17 shown the coexistence of vapour-liquid phases for the generic square well fluids under the slit-shaped confinements [26].
18 Presently, the silica pore is confined in the z-direction at the mentioned H values, with a constant pore surface area of 100
19 $\times 70\text{Å}^2$ in the x-y plane. The silica surfaces have been created in Visual Molecular Dynamics (VMD) software; starting
20 from an amorphous silica structure, similar to that reported by Jing et al. [35], with the each surface having a thickness of
21 5.54Å. The silica surface is further prepared by removing the top silicon atoms and passivating the non-bridging oxygen
22 atoms by hydrogen atoms, as reported by Farnandez et al. [36]. The passivation of a silica surface has been performed in
23 Quantum ATK® software; which resulted in 867 number of Si atoms, 2023 number of oxygen atoms and 633 number of
24 hydrogen atoms on the silica surface and thus saturating all the unfilled Si-bonds of the surface with hydroxyl (–OH)
25 groups (Figures 1a and 1b). Two such passivated silica surfaces are placed parallelly to each other at aforementioned
26 distances (H), with the –OH groups attached top surfaces forming the adsorbing sites for CO_2 in the slit geometry, as
27 shown in Figure 1c. Similar slit pore geometry with silica surfaces having attached –OH groups is recently studied by

researcher for adsorption and diffusivity estimations of confined propane inside silica pore [38]. The complete slit pore geometry is then geometry-optimised through the energy minimisation route in Quantum ATK®. Thus, the porous silica slit geometries with different H values include 1734 number of Si atoms, 4046 number of oxygen atoms and 1267 number of passivating hydrogen atoms. The porous silica adsorbent has been modelled using the ClayFF force field [25] with the van der Waals interactions and the electrostatic interactions being described by the conventional 12-6 LJ potential and Coulomb's Law, similar to equations 1 and 2, respectively. All the van der Waals interaction parameters for the ClayFF model have been reported in Table 1. The point charges assigned on the silicon atoms, the oxygen atoms and on the hydroxyl-hydrogen atoms of the silica surface via the ClayFF model are correspondingly +2.100e, -1.050e and +0.425e [25]. The partial charge assigned to silicon and oxygen atoms in the ClayFF force field results in a lesser potential well depth and hence allowing more flexibility in the silica surface for similar equilibrium bond distance between silica and oxygen when compared to the full charge force field. The pore-fluid interactions are estimated using the Lorentz-Berthelot classical mixing rule (as given in equations 3 and 4), and the corresponding parameter values are also reported in Table 1.

$$\epsilon_{sf} = \sqrt{\epsilon_{ss} \epsilon_{ff}} \quad (3)$$

$$\sigma_{sf} = \frac{\sigma_{ss} + \sigma_{ff}}{2} \quad (4)$$

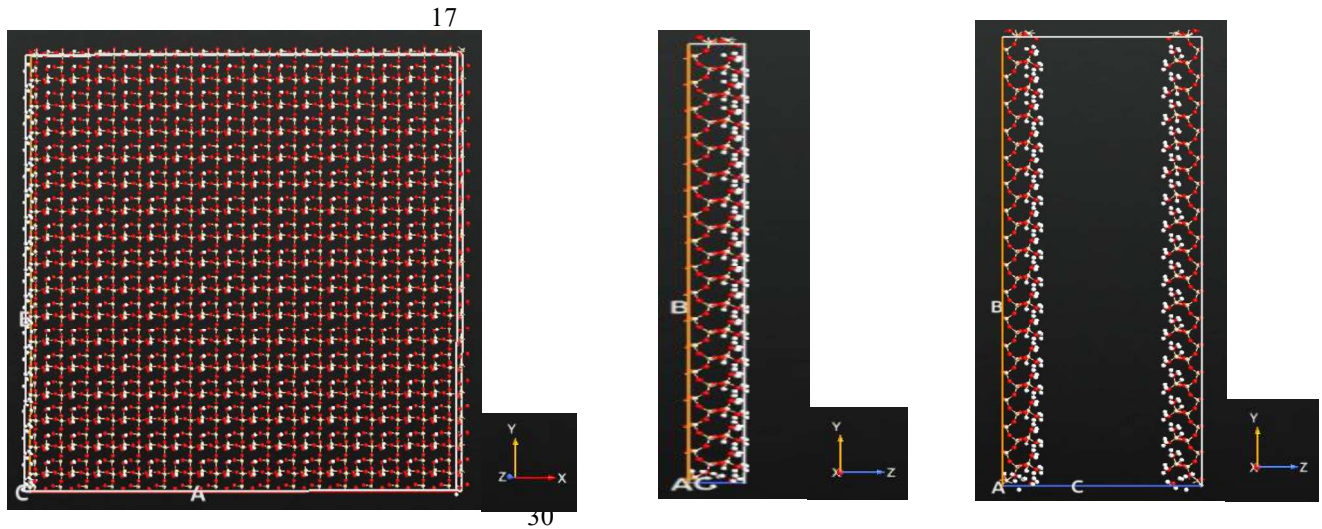


Figure 1: (a) Top view of a passivated silica surface; (b) Side view of a passivated silica surface; (c) Passivated silica slit pore. White dots representing passivating Hydrogen atoms, Red dots representing Oxygen atoms and Yellow dots representing Silicon atoms.

The open software package of MCCC-S-Towhee [27] has been deployed to conduct all the GCMC simulations for estimating the high temperature CO₂ adsorption isotherms inside the generated silica slit pores of variable slit height (H). All the Monte Carlo simulations in the Grand Canonical ensemble are equilibrated over 5×10⁵ steps, while the average property (adsorption data) has been calculated over the next 5×10⁵ steps. Probability moves for translation and addition/deletion of CO₂ molecules confined inside silica slit pores have been included during the GCMC simulations, in the ratio of

1 1:1; while the constituent atoms of the silica pore walls are held fixed with each wall having a thickness of 5.54Å. The
 2 standard deviations on all the estimated adsorption data are of 10^{-3} order after the equilibration of the system.

3 3. RESULTS

4 In this section we discuss on the calculated average bulk phase properties (e.g. densities, RDFs and chemical
 5 potentials) of CO₂ at temperatures 673.15K and 873.15K and within the methane steam reforming process pressure range
 6 of 500kPa to 4000kPa. We also present the estimated adsorption isotherms at the same thermodynamic conditions for
 7 confined CO₂ inside porous silica slit pores of various heights and draw a comparison with the existing data reported in
 8 literature for CO₂ adsorption inside porous carbon-based adsorbents. Furthermore, we present the local density plots of the
 9 confined CO₂ inside silica slit pores to understand the possibility of vapour-liquid phase equilibrium (VLE) inside the
 10 pores.

11 3.1 Bulk phase CO₂ properties

12 Initially, using the TraPPE force field (as described in Section 2) simulations in the Isothermal-Isobaric ensemble
 13 are performed to calculate the CO₂ densities at 673.15K and 873.15K over a pressure range of 500kPa to 4000kPa. The
 14 calculated bulk CO₂ densities are reported in Table 2, which show an excellent agreement with the corresponding
 15 experimental values from the literature [37].

16 Table 2: Simulated bulk CO₂ densities (ρ_b) from this work and the corresponding experimental values from the literature.

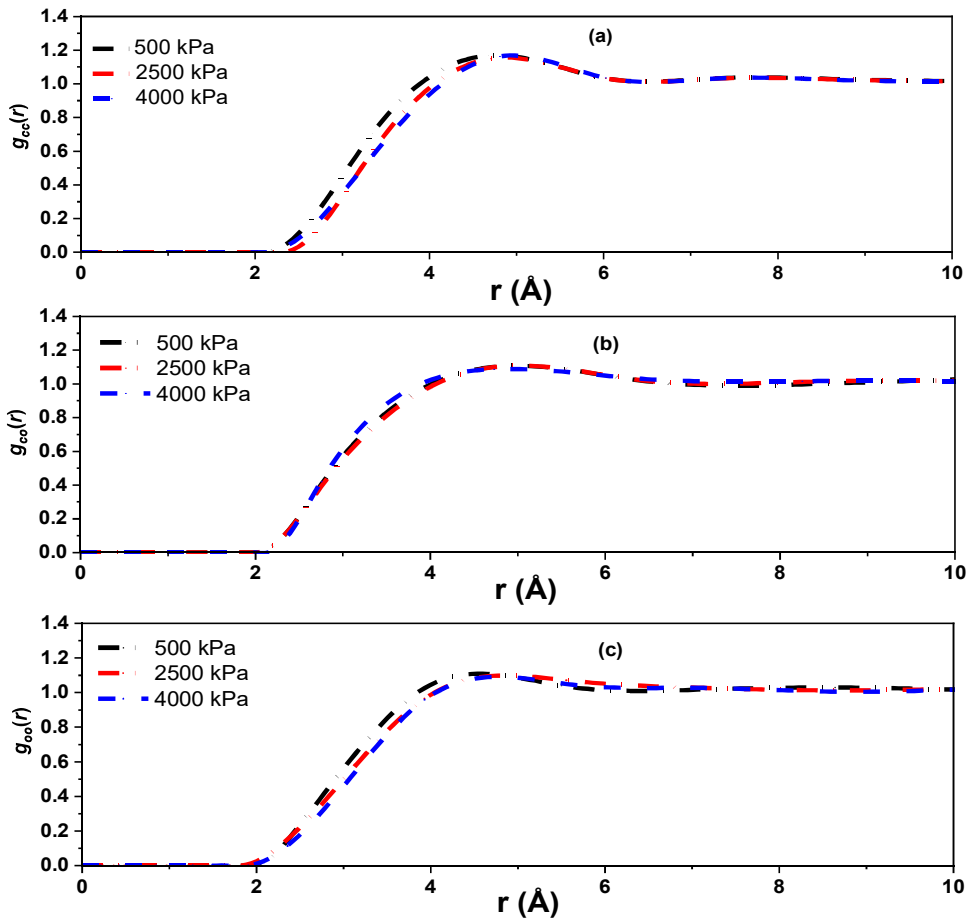
17 * % deviation = $\left(\frac{\text{experimental value} - \text{simulation value}}{\text{experimental value}} \right) \times 100$

T = 673.15K				T = 873.15K		
ρ_b (mmol·cm ⁻³)				ρ_b (mmol·cm ⁻³)		
P (kPa)	Present work	Span et al. [37]	% deviation	Present work	Span et al. [37]	% deviation
500	0.0893	0.0894	0.112	0.0688	0.0688	0
1000	0.1787	0.1788	0.056	0.1375	0.1375	0
1500	0.2680	0.2683	0.112	0.2060	0.2062	0.097
2000	0.3575	0.3579	0.112	0.2745	0.2747	0.073
2500	0.4466	0.4474	0.179	0.3428	0.3431	0.087
3000	0.5359	0.5371	0.224	0.4110	0.4113	0.073
3500	0.6253	0.6267	0.224	0.4790	0.4795	0.104
4000	0.7142	0.7164	0.308	0.5469	0.5476	0.128

18 The average volume obtained from the Isothermal-Isobaric ensemble simulations are used to estimate the RDFs and
 19 calculate the chemical potential values of the bulk CO₂ at these thermodynamic conditions via the MC simulations in
 20 Canonical ensemble. Figures 2 and 3 show the RDF ($g_{xy}(r)$, where x and y are the two atoms in the CO₂ molecules

1 separated by a distance r) plots at 673.15K and 873.15K temperatures for 500kPa, 2500kPa and 4000kPa pressures. It has
 2 been noted from all the RDF plots that for every temperature and pressure condition considered; the $g_{cc}(r)$, $g_{oo}(r)$ and $g_{co}(r)$
 3 reaches unity after the first peak; thus representing the gas phase bulk CO₂ at these thermodynamic conditions. Significant
 4 changes in the RDF peak heights are not observed with variations in the pressure and temperature. The position of
 5 occurrence for the first RDF peak at these temperature and pressure conditions are tabulated in Table 3. These values are in
 6 close compliance with the reported data in literature where the CO₂ molecule had been modelled using EPM [22]. The
 7 calculated chemical potential values for the bulk CO₂ obtained from the Canonical ensemble MC simulations using the
 8 Widom's insertion technique; shows an expected increase with an increase in pressure at a given temperature (refer Figure
 9 4).

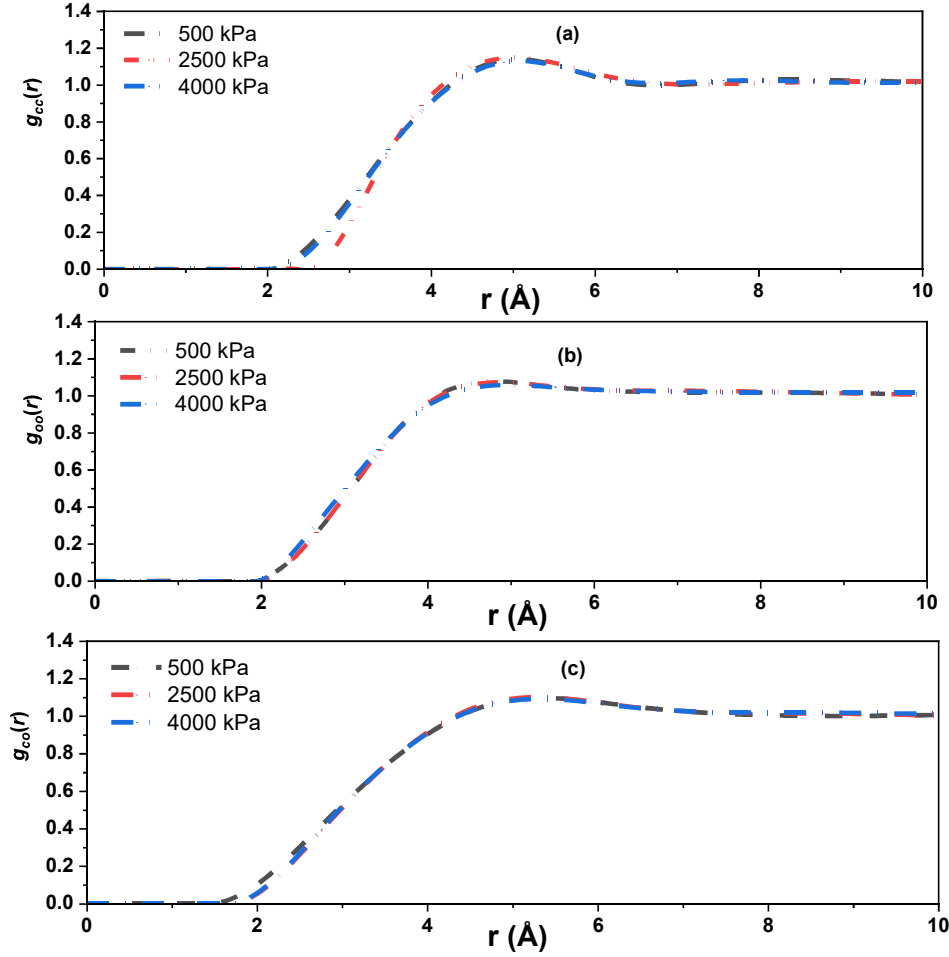
10



11

12 **Figure 2:** RDFs of bulk phase CO₂ at 673.15 K. (a) C-C RDF of CO₂ molecules; (b) C-O RDF of CO₂ molecules; (c) O-O
 13 RDF of CO₂ molecules.

14

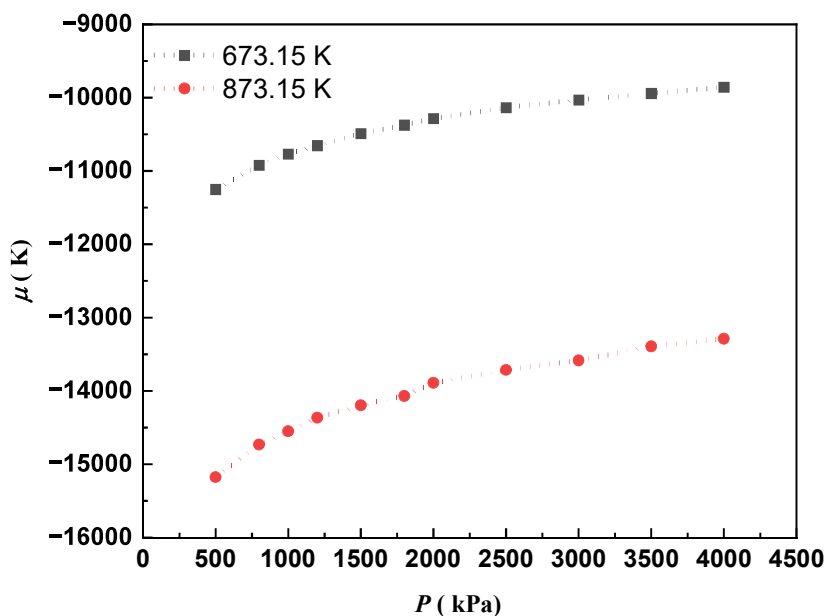


1
 2 **Figure 3:** RDFs of bulk phase CO₂ at 873.15 K. (a) C-C RDF of CO₂ molecules; (b) C-O RDF of CO₂ molecules; (c) O-O
 3 RDF of CO₂ molecules.
 4

5 **Table 3:** CO₂ RDF peak for $g_{cc}(r)$, $g_{co}(r)$, and $g_{oo}(r)$ at 673.15 K and 873.15 K at different pressures.

RDFs at 673.15K	500 kPa	2500 kPa	4000 kPa
$g_{cc}(r)$	4.68 Å	4.70 Å	4.81 Å
$g_{co}(r)$	5.50 Å	5.56 Å	5.62 Å
$g_{oo}(r)$	4.58 Å	4.65 Å	4.72 Å
RDFs at 873.15K	500 kPa	2500 kPa	4000 kPa
$g_{cc}(r)$	4.81 Å	4.83 Å	4.88 Å
$g_{co}(r)$	5.50 Å	5.52 Å	5.53 Å
$g_{oo}(r)$	4.58 Å	4.60 Å	4.63 Å

6
 7
 8

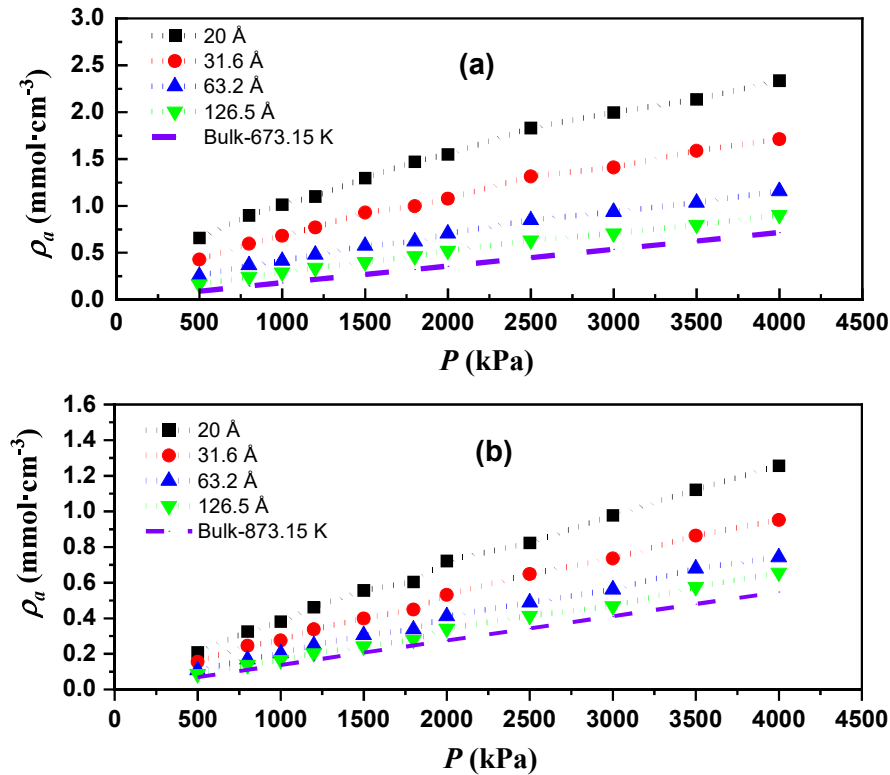


1
2 **Figure 4:** Variations in the chemical potential (μ) of bulk phase CO₂ with pressure at (a) 873.15 K; (b) 673.15K.

3
4
5 **3.2 CO₂ isotherms inside silica slit pores**

6
7 Traditional GCMC simulations have been carried out to generate adsorption isotherm data of confined CO₂ inside
8 silica pores of various slit heights ranging between 20Å and 126.5Å, using the calculated chemical potential values at the
9 high temperatures of 673.15K and 873.15K and over the pressure range of 500 – 4000kPa. Figure (5) shows the adsorption
10 isotherms inside the silica slit pores, with the adsorption surfaces saturated with –OH group, at 673.15K (Figure 5a) and at
11 873.15K (Figure 5b). The adsorption capacity of CO₂ by this porous silica, as expected, has been found to increase as the
12 loading pressure increases and the adsorption density decreases with an increase in the operating temperature. From Figure
13 (5) we also note that the uptake capacity of CO₂ inside porous silica-based material decreases with an increase in slit height;
14 which is due to the fact that, as shown in previous researches [28-30], inside smaller slit pore the pore-fluid interactions
15 (which is the function of r_{ij} , as described in Section 2) effectively spans over the complete pore height (H) than that inside
16 larger slit pores. It have been observed that the adsorption density (ρ_a) reaches to 0.161mmol.cm⁻³ from 0.659mmol.cm⁻³
17 and to 0.087mmol.cm⁻³ from 0.201mmol.cm⁻³ as the H is increased from 20Å to 126.5Å at T = 673.15K and 873.15K,
18 respectively, at 500kPa pressure; while the bulk phase densities of CO₂ at these operating conditions are 0.0893mmol.cm⁻³
19 and 0.0688mmol.cm⁻³, respectively, representing the supercritical state [22] (refer Table 2). Kumamuru et al. [22] had

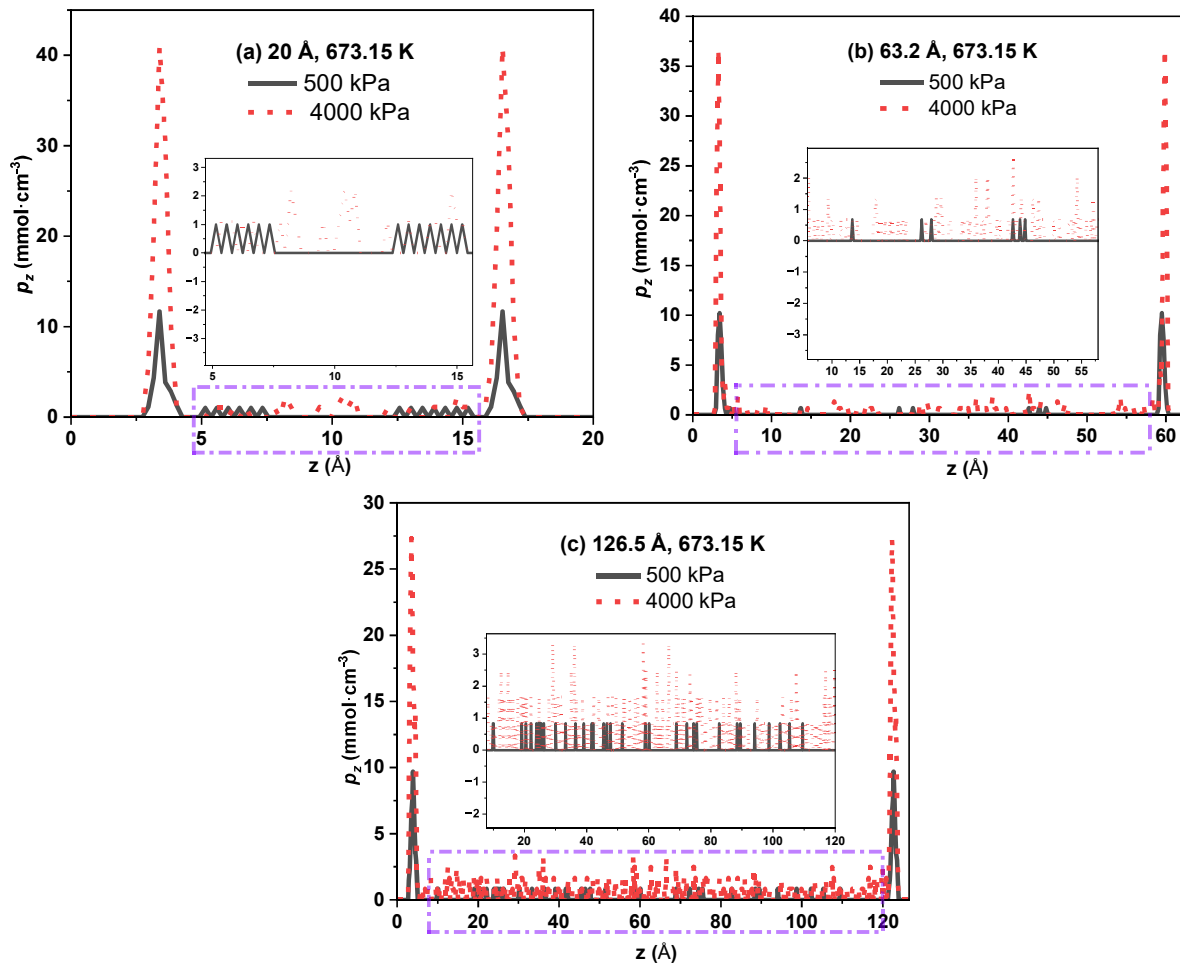
1 observed the similar trends in adsorption isotherms of CO₂ inside graphitic slit pores with same H values; however, in the
 2 present work we observe a higher adsorption inside the silica slit pores at the same thermodynamic pressure and
 3 temperature conditions. When compared to the CO₂ adsorption in graphitic slit pores [22], at T = 673.15K and P = 500kPa,
 4 the adsorption isotherms of CO₂ inside silica pores depicts a 1.5 times to almost 3.5 times enhancement of uptake as H
 5 decreases from 126.5Å to 20Å; while at 4000kPa and at the same temperature the increase in CO₂ uptake capacity in
 6 porous silica as compared to porous carbon is only about 1.12 to 1.66 times, respectively, as H decreases from 126.5Å to
 7 20Å. As expected, an increase in temperature to 873.15K reduces the CO₂ uptake capacity even in porous silica (as shown
 8 in Figure 5b); however the maximum adsorption is still observed in 20Å silica pore at 4000kPa, which is 1.257mmol.cm⁻³,
 9 as compared to 0.7935mmol.cm⁻³ that is observed in the porous carbon at same temperature and pressure conditions. This
 10 increased adsorption inside the silica slit pores compared to homogeneous carbon slit pore is attributed to the increased
 11 pore-fluid interactions between the adsorbed CO₂ and the silica slit pore with hydrogen-passivated adsorption surfaces
 12 (refer Table 1) compared to the pore-fluid interactions present between the carbon pore and the adsorbed CO₂ in it [22].
 13 The increased adsorption of CO₂ inside the silica slit pore compared to the carbon slit pore is in agreement to the argument
 14 made by Tenney and Lastoskie [19], where the researchers had shown that the increase in the oxygen-containing functional
 15 group on the chemically modified graphite pore wall further increased the adsorption capacity for CO₂ at a lower
 16 temperature; due to higher pore-fluid interactions.
 17



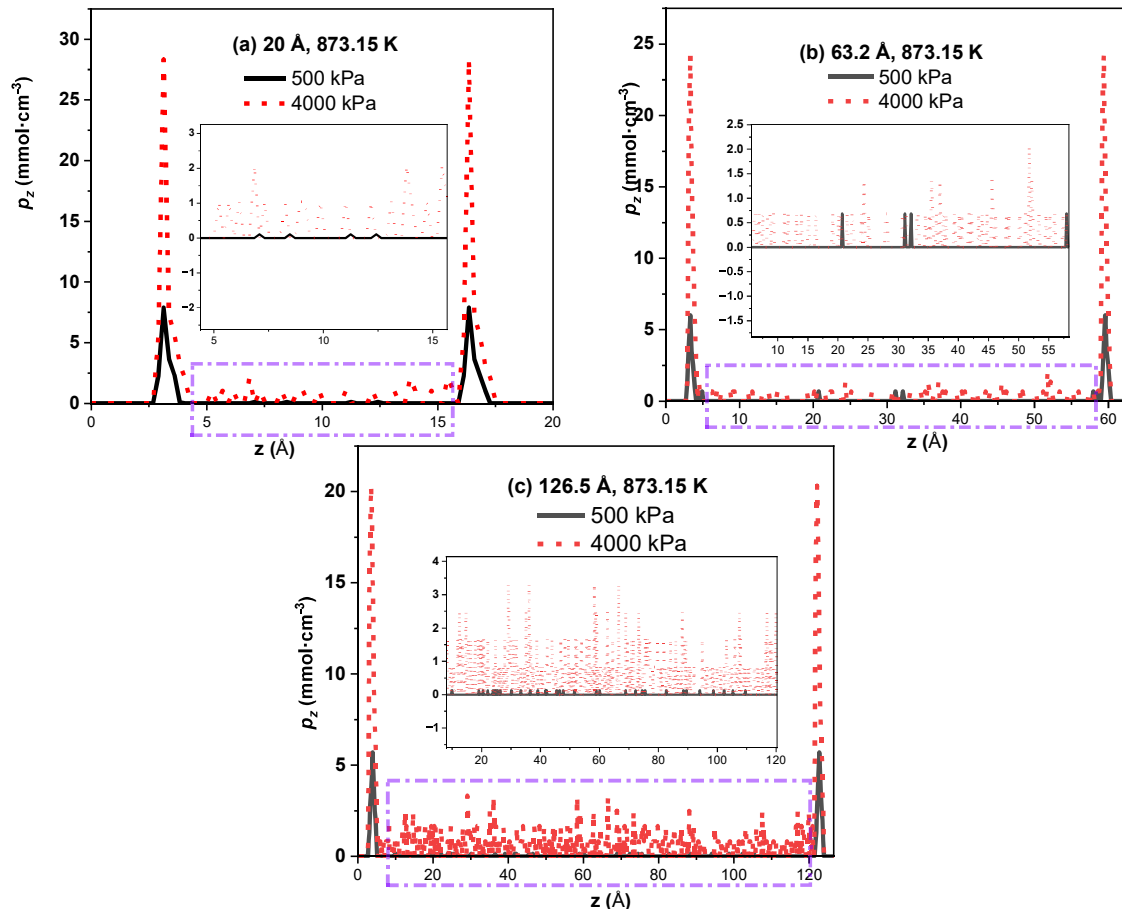
18
 19 **Figure 5:** Adsorption isotherms of CO₂ in silica slit pores (a) at 673.15 K and (b) at 873.15 K. The bulk density has been
 20 adapted from the reported data in literature [22].
 21

3.3 Molecular Packing of CO₂ inside silica slit pores

The structure properties of CO₂ are given by the local density profiles which provide the relevant information about the arrangement and molecular packing of the CO₂ molecules under the effect of confinement in the z direction along slit height (H). The structure properties of CO₂ confined inside porous silica with hydrogen-passivated adsorption surfaces and of various H at different temperature and pressure conditions are shown in Figures (6) and (7), where the local density varies as a function of z-direction. We note from Figures (6) and (7) that there are two high density peaks near the pore walls for all the porous silica slit pores considered, which is termed as layering in literature [16, 17], whereas the average local density at the centre of all the pores corresponds close to the particular bulk phase CO₂ densities at these given thermodynamic conditions (refer Figure 5 and Table 2 for bulk densities). Thus, the confined CO₂ inside all the slit pores considered in this study and at all the thermodynamic conditions; shows liquid-like packing behaviour near the pore walls compared to the pore centre, where the confined fluid shows more vapour-like behaviour resulting in the existence of VLE. Similar layering effects have also been reported for generic square well fluids [26] and generic triangle well fluids [31] confined inside attractive slit pores. Also, at a low temperature of 308K and at a pressure of 35bar; confined CO₂ showed similar liquid-like molecular packing near the pore walls and vapour-like phase at the pore centre of microporous carbons [18]. It is also observed from Figures (6) and (7) that with increase in pressure, the peak heights near the pore wall is increased; which corresponds to increasing adsorption with increase in pressure as can be seen from the adsorption isotherms (refer Figure 5); and also because of the lesser adsorption at higher temperature the layer peak height shows a decrease as the temperature increases from 673.15K to 873.15K. The study on CO₂ adsorption inside carbon slit pores at the 673.15K and 4000kPa [22] had shown the formation of two layers, one near each pore wall, and with a small incipient layer at the centre of 20Å slit pore. However, such an incipient layer is not observed in the present silica slit pore of 20Å at 673.15K and 4000kPa; while more liquid-like molecular packing of confined CO₂ towards the walls of the attractive silica pores (higher pore-fluid interactions compared to carbon pores, refer Table 1) has been noted. Also, the peak heights of these layers formed near the walls of 20Å silica slit pore at 4000kPa pressure, are close to 7.68 times higher than that inside the carbon slit pore of same dimension; thus, inferring higher adsorption and molecular packing of CO₂ inside silica slit pores compared to homogeneous carbon slit pores at same thermodynamic conditions of loading. Similar effect of increase in the pore-fluid interactions, on the formation of structured layers near the pore walls, has been also reported for krypton confined inside slit pores with different pore-fluid interaction values [32]. It is also observed from the density profile plots at both 673.15K and 873.15K that the peak height decreases with increase in H, which is in concurrent agreement with the adsorption isotherm data as shown in Figure 5. Kumamuru et al. [22] have reported the similar trends of layering in the local density profiles of CO₂ adsorbed inside carbon slit pores of same dimensions and at same thermodynamic conditions.



1
 2 **Figure 6.** One dimensional local CO₂ density profile along z direction in (a) 20Å (b) 63.2Å and (c) 126.5Å pore height at
 3 673.15 K.
 4
 5



1
2 **Figure 7.** One dimensional local CO₂ density profile along z direction in (a) 20Å (b) 63.2Å and (c) 126.5Å pore height at
3 873.15 K.

4
5
6 **4. CONCLUSION**

7
8 Molecular simulations have been carried out in the Isothermal-Isobaric ensemble, Canonical ensemble and in the
9 Grand Canonical ensemble for the present study, to estimate the bulk phase properties of CO₂ along with the CO₂
10 adsorption isotherms and the local density profiles inside silica slit pores at elevated temperatures over pressure ranging
11 from 500kPa to 4000kPa; which are the process parameters of steam reformation process for methane. From this study we
12 summaries the following:

- 13 (a) TraPPE force field adequately represents the CO₂ bulk properties at the aforementioned thermodynamic
14 conditions. We found that the bulk densities, RDFs and the chemical potential values are in excellent agreement
15 with that reported in literature [22, 37].
- 16 (b) Evidently, we note that the pore-fluid interactions between the CO₂ molecule and the silica pore are higher
17 compared to the pore-fluid interactions between homogeneous carbon pore and the CO₂ molecule [22]. Thus,
18 resulting in a higher CO₂ capture inside the silica pores as compared to porous carbon adsorbents.
- 19 (c) Adsorption capacity inside a porous silica adsorbent is greatly dependant on pore size (slit height, H, in this study)
20 along with the prevailing thermodynamic conditions. Interestingly, we observe higher uptake capacity of CO₂

1 inside smaller silica pores compared to the larger silica pores at a given thermodynamic condition. This is mainly
2 due to higher molecular packing of confined CO₂ inside smaller silica slit pores compared to the larger silica slit
3 pores, as shown by the higher peak heights of the layers formed near the slit walls for a smaller silica pore (Figure
4 **6a** and **7a**).

5 (d) We also observe that an increase in H results in a gradual shift of the ρ_a values towards the bulk phase density of
6 the CO₂ at that given thermodynamic conditions. Thus, the highest effect of the pore-fluid interactions are felt by
7 the adsorbate inside smaller silica pores, resulting in the possibility of higher CO₂ capture inside smaller slit pores.

8 (e) Finally, we note the coexistence of liquid-like (layers with high peak local density values) and vapour-like (local
9 **density values close to** corresponding local bulk phase densities) phase densities of CO₂ confined inside silica slit
10 pores at thermodynamic conditions where although the bulk phase CO₂ behaves supercritical.

11
12 **Acknowledgement:** Authors want to acknowledge DST-SERB and Indian Institute of Technology, Jodhpur for providing
13 necessary infrastructural supports and research facilities to conduct this work. This study is an outcome to the SERB
14 project number SRG/2019/000075.

15 **References:**

- 16 [1] U.S. Environmental Protection Agency, *Inventory Of U.S. Greenhouse Gas Emissions And Sinks: 1990–2014.*, 2016,
17 Washnigton, U.S.A
18 [2] Kohl, A. and Nielsen, R., *Gas Purification*, 1997, Houston, U.S.A
19 [3] Ahmed, Al-M.; Krishnamurthy, M.; Ali, A. R. and Rezaei, F., *Carbon Capture And Utilization Update*. Energy
20 Technology, 2017, 5, 834 – 849
21 [4] Wu, X.; Yu, Y.; Qin, Z. and Zhang, Z., *The Advances Of Post-Combustion CO₂ Capture With Chemical*
22 *Solvents: Review And Guidelines*. Energy Procedia, 2014, 63, 1339-1346.
23 [5] Bonenfant, D.; Mimeault, M. and Hausler, R., *Estimation Of The CO₂ Absorption Capacities In Aqueous 2-(2-*
24 *Aminoethylamino) Ethanol And Its Blends With MDEA And TEA In The Presence Of SO₂*. Ind. Eng. Chem. Res., 2007,
25 46, 8968-8971.
26 [6] van Holst, J.; Versteeg, G.; Brilman, D. and Hogendoorn, J., *Kinetic Study Of CO₂ With Various Amino Acid Salts*
27 *In Aqueous Solution*. Chem. Eng. Sci., 2009, 64, 59-68.
28 [7] Øi, L. and Kvan, S., *Comparison Of Energy Consumption For Different CO₂ Absorption Configurations Using*
29 *Different Simulation Tools*. Energy Procedia, 2014, 63, 1186-1195.
30 [8] Amanda, A.; Moral-Vico, J.; Markeb, A.; Busquets-Fite, M.; Komilis, D.; Puentes, V.; Sanchez, A. and Font, X.,
31 *Critical Review Of Existing Nanomaterial Adsorbents To Capture Carbon Dioxide And Methane*. Sci. Total. Environ,
32 2017, 595, 51-62.
33 [9] Younas, M.; Sohail, M.; Leong, L.; Bashir, M. and Sumathi, S., *Feasibility Of CO₂ Adsorption By Solid*
34 *Adsorbents: A Review On Low-Temperature Systems*. Int. J. Environ. Sci. Technol., 2016, 13, 1839-1860.
35 [10] Murge, P.; Dinda, S. and Roy, S., *Zeolite-Based Sorbent For CO₂ Capture: Preparation And Performance*
36 *Evaluation*. Langmuir, 2019, 35, 14751-14760.
37

- 1 [11] Dinda, S.; Murge, P. and Chakravarthy, B., *A Study On Zeolite-Based Adsorbents For CO₂ Capture*. Bull. of Mater.
2 Sci., 2019, 42, 240.
- 3 [12] Murge, P.; Dinda, S. and Roy, S., *Adsorbent From Rice Husk For CO₂ Capture: Synthesis, Characterization And*
4 *Optimization Of Parameters*. Energy fuels, 2018, 32, 10786–10795.
- 5 [13] Levesque, D. and Lamari, F., *Pore Geometry And Isotheric Heat: An Analysis Of Carbon Dioxide Adsorption On*
6 *Activated Carbon*. Mol. Phys., 2009, 107, 591-597.
- 7 [14] Kirchofer, A.; Firouzi, M.; Psarras, P. and Wilcox, J., *Modeling CO₂ Transport And Sorption In Carbon Slit*
8 *Pores*. J. Phys. Chem. C, 2017, 121, 21018–21028.
- 9 [15] Jasuja, H. and Walton, K. S., *Experimental Study Of CO₂, CH₄, And Water Vapor Adsorption On A Dimethyl-*
10 *Functionalized Uio-66 Framework*. J. Phys. Chem. C, 2013, 117, 7062–7068
- 11 [16] Steriotis, T.; Papadopoulos, G.; Stubos, A. and Kanellopoulos, N., *A Monte Carlo Study On The Structure Of*
12 *Carbon Dioxide Adsorbed In Microporous Carbons*. Stud. Surf. Sci. Catal., 2002, 144, 545-552.
- 13 [17] Balbuena, P. B. and Gubbins, K. E., *Classification Of Adsorption Behavior: Simple Fluids In Pores Of Slit*
14 *Shaped Geometry*. Fluid Phase Equilibria, 1992, 76, 21-35.
- 15 [18] Samios, S.; Papadopoulos, G.; Steriotis, T. and Stubos, A., *Simulation Study Of Sorption Of CO₂ And N₂ With*
16 *Application To The Characterization Of Carbon Adsorbents*. Mol. Simul., 2001, 27, 441-456.
- 17 [19] Tenney, C. M. and Lastoskie, C. M., *Molecular Simulation Of Carbon Dioxide Adsorption In Chemically And*
18 *Structurally Heterogeneous Porous Carbons*. Environ. Prog., 2006, 25, 343-354.
- 19 [20] Lithoos, G.; Peristeras, L.; Boulougouris, G. and Economou, I., *Monte Carlo Simulation Of Carbon Monoxide,*
20 *Carbon Dioxide And Methane Adsorption On Activated Carbon*. Mol. Phys., 2012, 110, 1153-1160.
- 21 [21] Kurniawan, Y.; Bhatia, S. and Rudolph, V., *Simulation Of Binary Mixture Adsorption Of Methane And CO₂ At*
22 *Supercritical Conditions In Carbons*. AIChE J., 2006, 52, 957-967.
- 23 [22] Kumamuru, N. B.; Sengupta, A. and Dinda, S., *Molecular Simulation Study Of CO₂ Adsorption In Carbon Slit*
24 *Pores At High Temperature And Pressure Conditions*. Bull Mater Sci., 2020, 43, 296.
- 25 [23] Frenkel, D. and Smit, B., *Understanding Molecular Simulation From Algorithms To Applications*. San Diego:
26 Academic Press, 1996.
- 27 [24] Harris, J. and Yung, K., *Carbon Dioxide's Liquid-Vapor Coexistence Curve And Critical Properties As Predicted*
28 *By A Simple Molecular Model*. J. Phys. Chem., 1995, 99, 12021-12024.
- 29 [25] Cygan, R. T.; Liang, J. and Kalinichev, A. G., *Molecular Models Of Hydroxide, Oxyhydroxide, And Clay Phases*
30 *And The Development Of A General Force Field*. J. Phys. Chem. B, 2004, 108, 1255–1266.
- 31 [26] Singh S. K.; Saha, A. K. and Singh, J. K., *Molecular Simulation Study Of Vapor-Liquid Critical Properties Of A*
32 *Simple Fluid In Attractive Slit Pores: Crossover From 3D To 2D*. J. Phys. Chem. B., 2010, 114, 4283–4292.
- 33 [27] Martin, M., *MCCCS Towhee: A Tool For Monte Carlo Molecular Simulation*. Mol. Simul., 2013, 39, 1212-1222.
- 34 [28] Abraham, F. F., *The Interfacial Density Profile Of A Lennard-Jones Fluid In Contact With A (100) Lennard-Jones*
35 *Wall And Its Relationship To Idealized Fluid/Wall Systems: A Monte Carlo Simulation*. J. Chem. Phys., 1978, 68, 3716 –
36 3716.
- 37 [29] Evans, R. and Marini, B. M. U., *Phase Equilibria And Solvation Forces For Fluids Confined Between Parallel*

- 1 *Walls*. J. Chem. Phys., 1987, 86, 7138 – 7148.
- 2 [30] Cabria I., *Comparison Of Theoretical Methods Of The Hydrogen Storage Capacities Of Nanoporous Carbons*. Intl. J.
- 3 Hydrogen Economy, 2021, 46, 12192 – 12205.
- 4 [31] Sengupta, A.; Behera, P. and Adhikari, J., *Molecular Simulation Study Of Triangle-Well Fluids Confined In Slit*
- 5 *Pores*. Mol. Phys., 2014, 112, 1969–1978.
- 6 [32] Sengupta, A. and Adhikari, J., *A Grand Canonical Monte Carlo Simulation Study Of Argon And Krypton Confined*
- 7 *Inside Weakly Attractive Slit Pores*. Mol. Simul., 2015, 41, 402 – 413.
- 8 [33] Chen, C.; Hu, W.; Li W. and Song, Y., *Model Comparison of the CH₄/CO₂/Water System in Predicting Dynamic and*
- 9 *Interfacial Properties*. J. Chem. Eng. Data., 2019, 64, 2464 – 2474.
- 10 [34] Vujic, B. and Lyubartsev, A. P., *Transferable force-field for modelling of CO₂, N₂, O₂ and Ar in all silica and Na⁺*
- 11 *exchanged zeolites*. Modelling Simul. Mater. Sci. Eng., 2016, 24, 26pp.
- 12 [35] Jing, Y.; Wei, L.; Wang, Y. and Yu, Y., *Molecular simulation of MCM-41: Structural properties and adsorption of*
- 13 *CO₂, N₂ and flue gas*. Chem. Eng. J., 2013, 220, 264 – 275.
- 14 [36] Farnandez-Farnandez, A. M.; Conde, M. M.; Perez-Sanchez, G.; Perez-Rodriguez, M. and Pineiro, M. M., *Molecular*
- 15 *simulation of methane hydrate growth confined into a silica pore*. J. Mol. Liquids, 2022, 362, 119698.
- 16 [37] Span, R. and Wagner, W., *A New Equation of State for Carbon Dioxide Covering the Fluid Region from the Triple-*
- 17 *Point Temperature to 1100 K at Pressures up to 800 MPa*. Phys. Chem. Ref. Data, 1996, 25, 1509 – 1596.
- 18 [38] Gautam, S.; Le, T.; Striolo, A. and Cole, D., *Molecular dynamics simulations of propane in slit shaped silica nano-*
- 19 *pores: direct comparison with quasielastic neutron scattering experiments*. Phys. Chem. Chem. Phys., 2017, 19, 32320.

Tables

Table 1: Molecular parameters used for CO₂ molecules and slit silica wall.

CO ₂		Silica wall		Pore-fluid parameters	
σ_{ff} (Å)	$k_B^{-1} \cdot \epsilon_{ff}$ (K)	σ_{ff} (Å)	$k_B^{-1} \cdot \epsilon_{ff}$ (K)	σ_{sf} (Å)	$k_B^{-1} \cdot \epsilon_{sf}$ (K)
$\sigma_{c-c} = 2.8000$	$k_B^{-1} \cdot \epsilon_{c-c} = 27.00$	$\sigma_{Si-Si} = 3.3020$	$k_B^{-1} \cdot \epsilon_{Si-Si} = 9.0 \times 10^{-4}$	$\sigma_{C-Si} = 3.0510$	$k_B^{-1} \cdot \epsilon_{C-Si} = 0.1580$
				$\sigma_{C-O} = 2.9820$	$k_B^{-1} \cdot \epsilon_{C-O} = 45.9490$
$\sigma_{c-o} = 2.9250$	$k_B^{-1} \cdot \epsilon_{c-o} = 46.1800$	$\sigma_{O-O} = 3.1655$	$k_B^{-1} \cdot \epsilon_{O-O} = 78.1200$	$\sigma_{O-O} = 3.1070$	$k_B^{-1} \cdot \epsilon_{O-O} = 78.5980$
$\sigma_{o-o} = 3.0500$	$k_B^{-1} \cdot \epsilon_{o-o} = 79.00$			$\sigma_{O-Si} = 3.2330$	$k_B^{-1} \cdot \epsilon_{O-Si} = 0.2690$
				$\sigma_{H-H} = 0$	$k_B^{-1} \cdot \epsilon_{H-H} = 0.$
				$\sigma_{H-O} = 1.5820$	$k_B^{-1} \cdot \epsilon_{H-O} = 0.$
				$\sigma_{H-Si} = 1.6510$	$k_B^{-1} \cdot \epsilon_{H-Si} = 0.$
				$\sigma_{H-C} = 1.4000$	$k_B^{-1} \cdot \epsilon_{H-C} = 0.$
				$\sigma_{H-O} = 1.5250$	$k_B^{-1} \cdot \epsilon_{H-O} = 0.$

Table 2: Simulated bulk CO₂ densities (ρ_b) from this work and the corresponding experimental values from the

literature. * % deviation = $\left(\frac{\text{experimental value} - \text{simulation value}}{\text{experimental value}} \right) \times 100$

T = 673.15K				T = 873.15K		
ρ_b (mmol·cm⁻³)				ρ_b (mmol·cm⁻³)		
P (kPa)	Present work	Span et al. [37]	% deviation	Present work	Span et al. [37]	% deviation
500	0.0893	0.0894	0.112	0.0688	0.0688	0
1000	0.1787	0.1788	0.056	0.1375	0.1375	0
1500	0.2680	0.2683	0.112	0.2060	0.2062	0.097
2000	0.3575	0.3579	0.112	0.2745	0.2747	0.073
2500	0.4466	0.4474	0.179	0.3428	0.3431	0.087
3000	0.5359	0.5371	0.224	0.4110	0.4113	0.073
3500	0.6253	0.6267	0.224	0.4790	0.4795	0.104
4000	0.7142	0.7164	0.308	0.5469	0.5476	0.128

Table 3: CO₂ RDF peak for $g_{cc}(r)$, $g_{co}(r)$, and $g_{oo}(r)$ at 673.15 K and 873.15 K at different pressures.

RDFs at 673.15K	500 kPa	2500 kPa	4000 kPa
$g_{cc}(r)$	4.68 Å	4.70 Å	4.81 Å
$g_{co}(r)$	5.50 Å	5.56 Å	5.62 Å
$g_{oo}(r)$	4.58 Å	4.65 Å	4.72 Å
RDFs at 873.15K	500 kPa	2500 kPa	4000 kPa
$g_{cc}(r)$	4.81 Å	4.83 Å	4.88 Å
$g_{co}(r)$	5.50 Å	5.52 Å	5.53 Å
$g_{oo}(r)$	4.58 Å	4.60 Å	4.63 Å

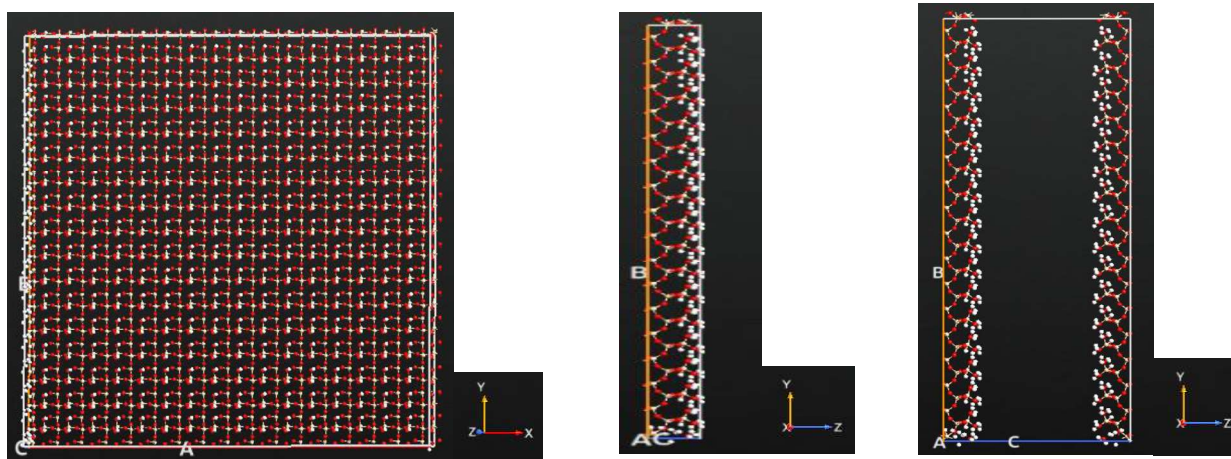
Figures

Figure 1: (a) Top view of a passivated silica surface; (b) Side view of a passivated silica surface; (c) Passivated silica slit pore. White dots representing passivating Hydrogen atoms, Red dots representing Oxygen atoms and Yellow dots representing Silicon atoms.

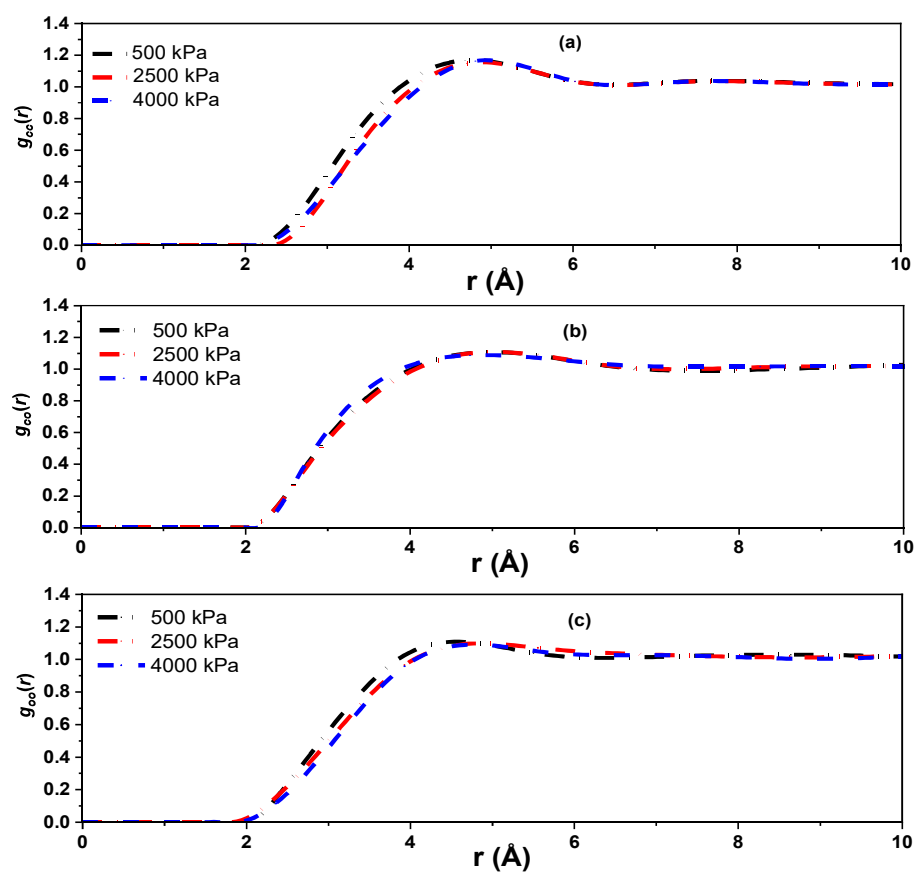


Figure 2: RDFs of bulk phase CO₂ at 673.15 K. (a) C-C RDF of CO₂ molecules; (b) C-O RDF of CO₂ molecules; (c) O-O RDF of CO₂ molecules.

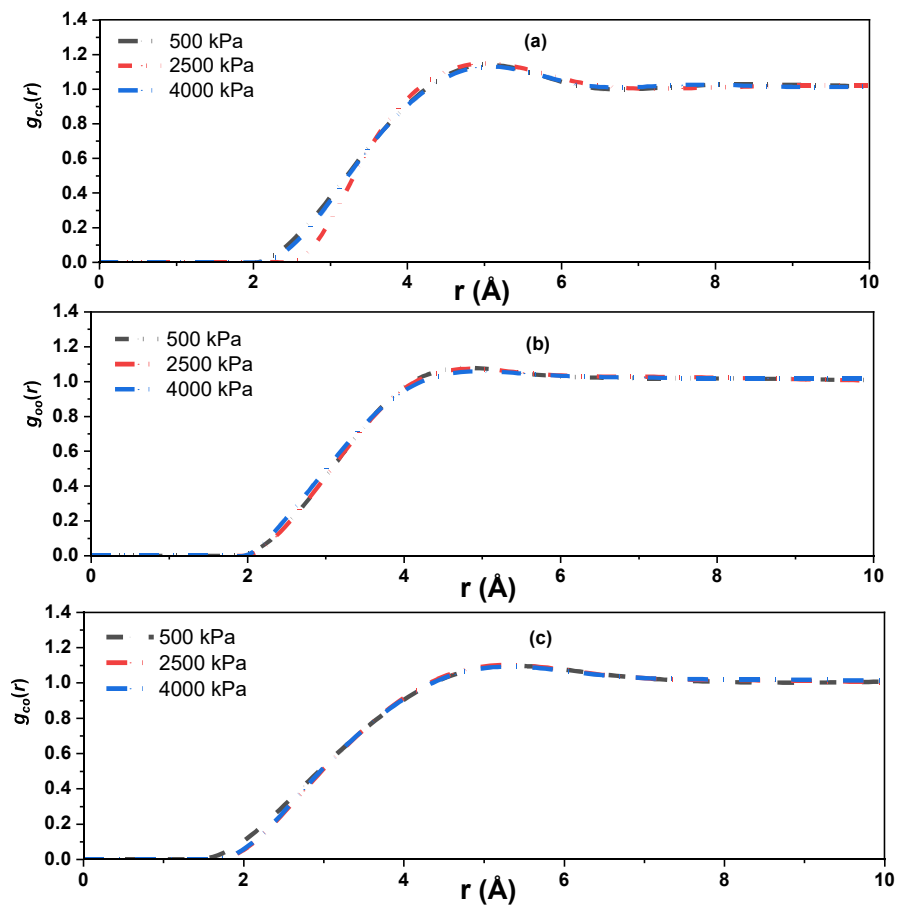


Figure 3: RDFs of bulk phase CO₂ at 873.15 K. (a) C-C RDF of CO₂ molecules; (b) C-O RDF of CO₂ molecules; (c) O-O RDF of CO₂ molecules.

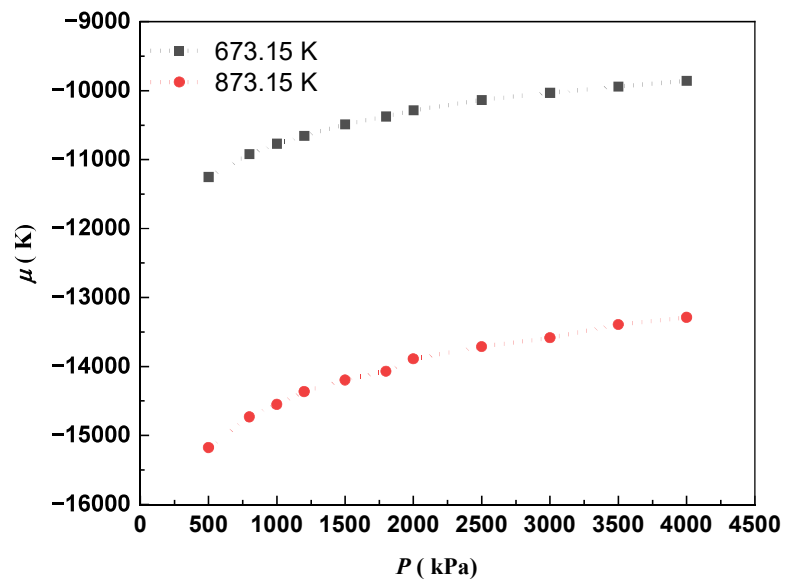


Figure 4: Variations in the chemical potential (μ) of bulk phase CO₂ with pressure at (a) 873.15 K; (b) 673.15K.

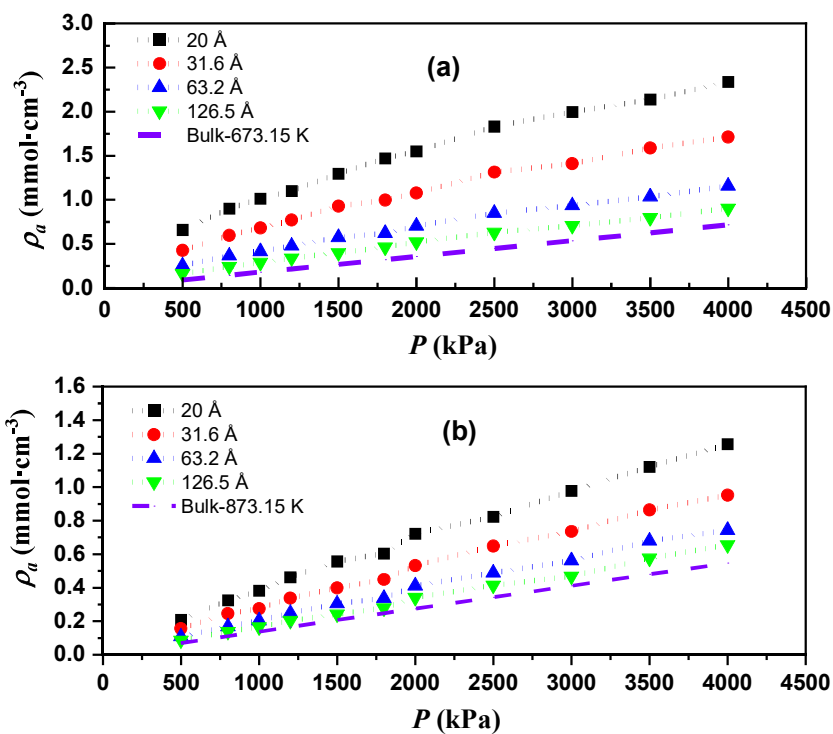


Figure 5: Adsorption isotherms of CO₂ in silica slit pores (a) at 673.15 K and (b) at 873.15 K. The bulk density has been adapted from the reported data in literature [22].

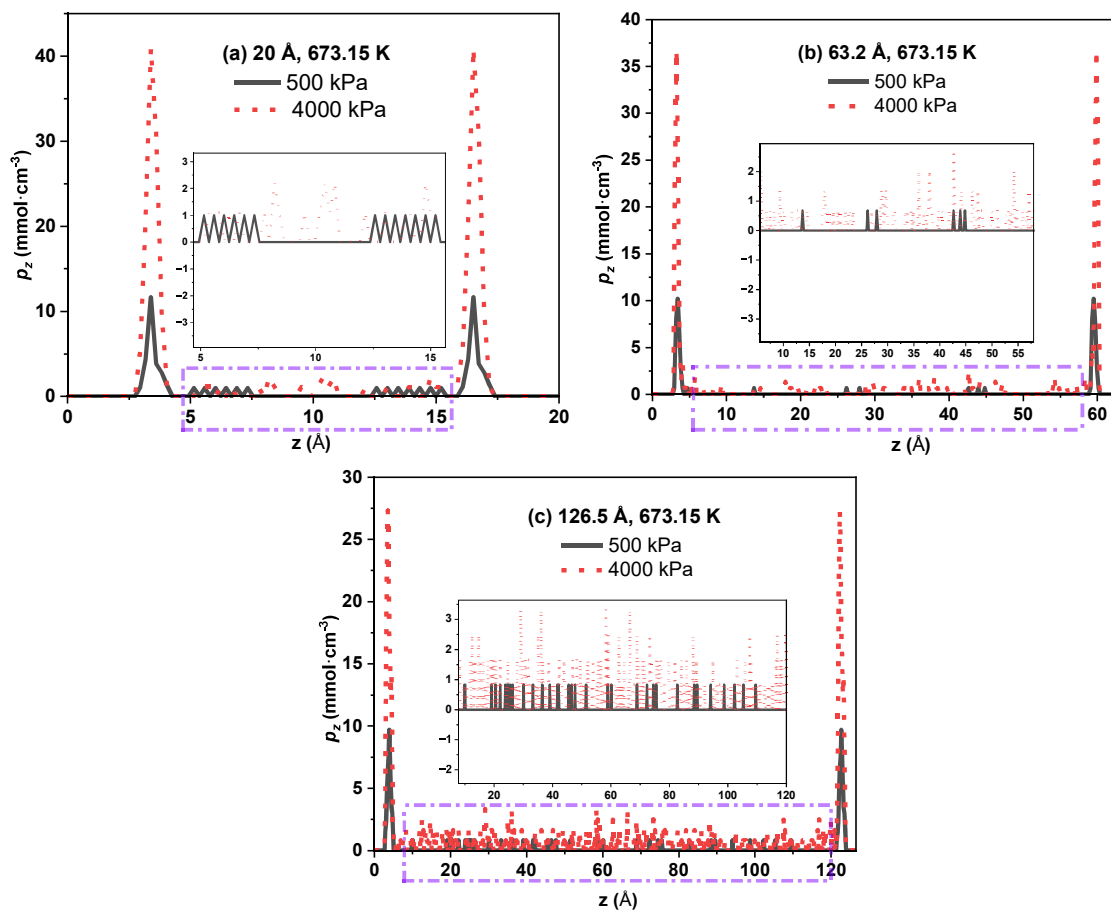


Figure 6. One dimensional local CO₂ density profile along z direction in (a) 20Å (b) 63.2Å and (c) 126.5Å pore height at 673.15 K.

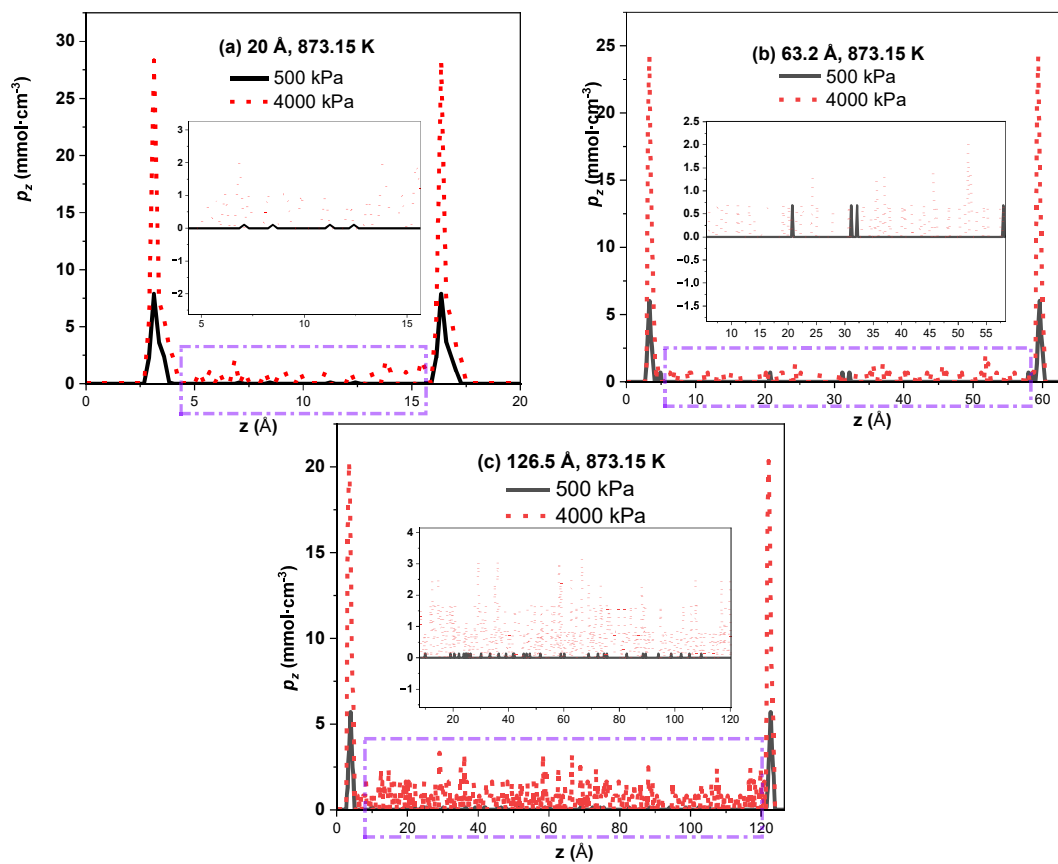


Figure 7. One dimensional local CO₂ density profile along z direction in (a) 20Å (b) 63.2Å and (c) 126.5Å pore height at 873.15 K.